Curable layered double hydroxide nanoparticles-based perfusion contrast agents for X-ray computed tomography imaging of vascular structures

Tokudome, Yasuaki; Poologasundarampillai, Gowsihan; Tashibana, Koki; Murata, Hidenobu; Naylor, Amy; Yoneyama, Akio; Nakahira, Atsushi

Link to publication on Research at Birmingham portal

RESEARCH ARTICLE

**ADVANCED
NANOBIOMED
RESEARCH**
Open Access

www.advnanobiomedres.com

Curable Layered Double Hydroxide Nanoparticles-Based Perfusion Contrast Agents for X-Ray Computed Tomography Imaging of Vascular Structures

Yasuaki Tokudome,* Gowsihan Poologasundarampillai,* Koki Tachibana, Hidenobu Murata, Amy J. Naylor, Akio Yoneyama, and Atsushi Nakahira

Imaging complex vascular structures by X-ray microcomputed tomography (μ-CT) is becoming vital for research purposes in pathology of vascular diseases. Acrylic-based polymerizable resins are widely adopted for the contrast agent to prepare pathological specimens for imaging of vascular structures. For imaging of vascular structures at higher resolution, it is promising to develop inorganic-type contrast agents with higher X-ray attenuation coefficient as well as low viscosity, homogeneity, minimum shrinkage, curable (gellable) for replication, and low cost. Herein, a novel inorganic sol–gel system based on concentrated colloidal dispersion of NiAl layered double hydroxide (LDH) nanoparticles is described, allowing imaging of vascular structures at high resolution. NiAl LDH acts as nanofiller and alkaline catalyst to form a silica/LDH monolithic material with homogeneity from the nanoscale. Moreover, NiAl LDH nanoparticles contribute to the strong enhancement of the X-ray attenuation. As a proof-of-concept, X-ray μ-CT imaging of the developed contrast agent in glass capillaries and of blood vessels of a human placenta and murine liver is demonstrated.

1. Introduction

Imaging is fundamental for unraveling the cellular and molecular mechanisms of life[1] and plays a major part in diagnosing disease and treatment planning. X-ray microcomputed tomography (μ-CT) provides detailed images of internal microstructure of organs such as bone, heart and blood vessels with a high spatial resolution.[2]

Imaging complex vascular structures by X-ray μ-CT is becoming vital for research purposes in pathology of vascular diseases. Since an image contrast of vascular structure against surrounding soft tissues is relatively small and therefore difficult to detect, contrast agents are employed by being perfused and cured into a solid inside blood vessels for the pathological examination. The development of contrast agents is therefore key to further the applicability of various imaging modalities.

Acrylic-based polymerizable resins have been widely adopted for the contrast agent to prepare pathological specimens for imaging of vascular structures.[3] Acrylic-based polymerizable resins meet several critical requirements, low viscosity, homogeneity, minimum shrinkage, curable (gellable) for replication, and low cost allowing imaging of whole organs and animals.[4] However, acrylic polymers also have low X-ray attenuation coefficient, meaning that they cannot be readily visualized with this method. To circumvent this problem, the surrounding tissue is dissolved (maceration) leaving behind the vascular casts which are then imaged.[4a,c,5] One major limitation of this method is that the fine capillaries can become damaged and lost during the maceration step, reducing the quality and integrity of the resulting vascular network images/data.

Inorganic nanomaterials containing metallic elements are highly promising as contrast agents to achieve a contrast toward high-resolution X-ray μ-CT, however, proven inorganic nanoparticles, such as noble metals, Ag, Au, Pt,[6a,7] are expensive and are required in large quantity to perfuse vasculature. Moreover, these inorganic nanoparticles may become aggregated, which results in blockages and hinders perfusion of small vessels and capillaries.[8]

To achieve the benefits of an inorganic-based contrast agent, while addressing the challenges outlined above, we assessed the suitability of layered double hydroxides (LDHs) as vascular

Y. Tokudome, K. Tachibana, H. Murata, A. Nakahira
Department of Materials Science
Graduate School of Engineering
Osaka Prefecture University
Sakai, Osaka 599-8531, Japan
E-mail: tokudome@mtr.osakafu-u.ac.jp

G. Poologasundarampillai
School of Dentistry
University of Birmingham
Birmingham B15 2TT, UK
E-mail: G.Poologasundarampillai@bham.ac.uk

A. J. Naylor
Institute of Inflammation and Ageing
University of Birmingham
Birmingham B15 2TT, UK

A. Yoneyama
SAGA Light Source
8-7 Yayoigaoka Tosu, Saga 841-0005, Japan

The ORCID identification number(s) for the author(s) of this article can be found under https://doi.org/10.1002/anbr.202100123.

**ADVANCED
SCIENCE NEWS**

www.advancedsciencenews.com

**ADVANCED
NanoBiomed
RESEARCH**
Open Access

www.advnanobiomedres.com

contrast agents. LDHs are a family of lamellar metal hydroxides accommodating anions in their interlayers, with a general formula of $[M^{2+}_{1-x}M^{3+}_x(OH)_2][A_{x/n}^{n-}\cdot mH_2O]$, where M^{2+} and M^{3+} are di- and trivalent cations, and A^{n-} is an anion. The flexibility of choice of constituent metal ions is advantageous to develop various types of contrast agents for bio-imaging. Examples include Gd-complex intercalated MgAl LDH[9] and MgMnAl LDH[10] for magnetic resonance imaging (MRI), and MgAl LDH accommodating near-infrared (NIR) fluorescent dyes for optical imaging.[11] Dual imaging via CT/MRI has also been reported on LDH-based composites of Gd(OH)₃/LDH[12] and Gd-doped MgAl LDH/Au.[13] Further sophisticated techniques for theranostic nanoplatforms (i.e., imaging-guided nanomedicine), have been reported using Cu-doped LDH nanoparticles,[14] MgMnAl LDH,[15] and GaZnAl LDH modified with chlorogenic acid and Au nanoparticles.[16] These existing materials are used in the form of diluted suspension of nanomaterials for injection, rather than as curable casts, indeed the diameter of the LDH nanoparticles, in the range of tens to hundreds of nm, is too large to form a stable gel in μm-scale homogeneity.

Recently, we have reported a synthesis of NiAl LDH nanoparticles with a diameter of 8 nm.[17] These nanometric LDHs can be obtained in the form of concentrated colloidal dispersion as high as 100 mg mL⁻¹ in ethanol. The unique surface chemistry, as well as the extremely small size, suggested that they could be integrated with an inorganic-based polymerization reaction to provide a novel curable resin, allowing for high-resolution X-ray μ-CT imaging.

Herein, we describe a novel inorganic sol–gel system based on concentrated colloidal dispersion of NiAl LDH nanoparticles, allowing high-resolution imaging of vascular structures (capillaries down to 5 μm) (**Figure 1**). Silicon alkoxides, tetraethoxysilane (TEOS), and methyltriethoxysilane (MTES), were used as a sol–gel crosslinker to interconnect NiAl LDH nanoparticles in the concentrated colloidal suspension. At 37 °C, the addition of H_2O triggers the formation of a nanoparticulate LDH gel. We established that NiAl LDH acts as nanofiller and alkaline catalyst to form a silica/LDH monolithic material with homogeneity from the nanoscale. Moreover, NiAl LDH nanoparticles contribute to the strong enhancement of the X-ray attenuation, to the extent that imaging of vascular structure is possible without maceration. As a proof-of-concept, we have demonstrated X-ray μ-CT imaging of the developed contrast agent in glass capillaries (20–100 μm in diameter) and of blood vessels of a human placenta and murine liver. This contrast agent is readily prepared and used and therefore provides a promising option for imaging, allowing high contrast, which has the potential to offer deeper insights into vascular pathology.

2. Results and Discussion

2.1. Development of Multicomponent Wetgels Employing Concentrated Dispersion of LDH Nanoparticles

The present material synthesis was inspired by our previous report on colloidal dispersion of LDH nanoparticles.[17] As described in the report, NiAl LDH nanoparticles ($d \approx 8$ nm) suspended in a solvent (≈ 100 mg mL⁻¹) was synthesized via a one pot liquid phase reaction. Even though the concentration of 100 mg mL⁻¹ is 10–100 times higher than standard LDH suspensions,[18] it was not enough to make a nanoparticulate robust gel with a considerable X-ray attenuation coefficient. Therefore, we first explored a route to concentrate the suspension and integrate with a silicon-alkoxide-derived sol–gel reaction. The suspension was freeze dried such that LDH nanoparticle powder could be collected without strong aggregation (Figure S2, Supporting Information). The freeze-dried LDH nanoparticles had a chemical composition of $Ni_2Al(OH)_6\cdot acac\cdot mCl\cdot nH_2O$ (acac: acetylacetone). It is interesting to note that the freeze-dried LDH can be homogeneously redispersed in EtOH at concentrations as high as 800 mg in 1 mL after mild heating to 50 °C. This high dispersion stability allowed us to explore curable contrast agent based on the nanometric LDH.

The contrast agent was designed as a mixture of TEOS and MTES as inorganic cross linkers, and NiAl LDH to provide: 1) a solid basic catalyst to drive hydrolysis and condensation reactions; 2) nanofiller to reinforce the gel networks; 3) X-ray attenuator to enhance the contrast. After the addition of H_2O to the mixture of TEOS, MTES, LDH in EtOH solvent, gelation was successfully induced at 37 °C for optimized chemical compositions (**Table 1** and Figure S3, Supporting Information). The samples
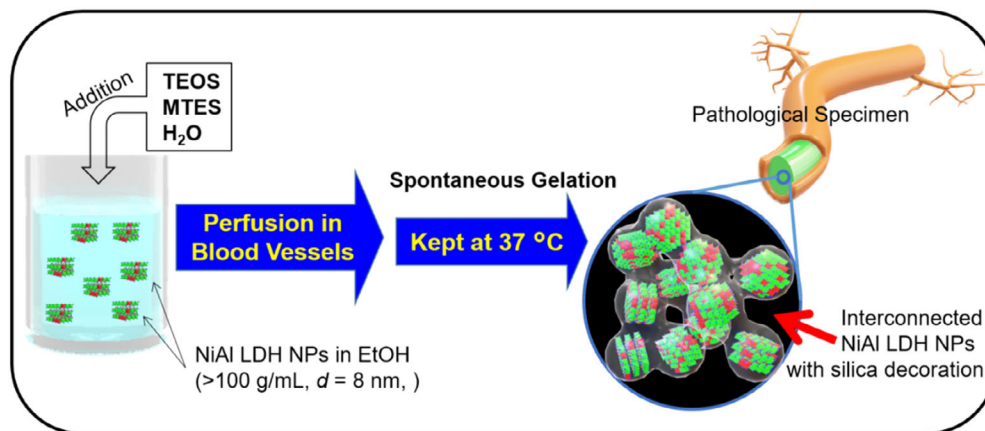

Figure 1. Schematic illustration showing the thermogellable contrast agent based on the concentrated dispersion of LDH nanoparticles.

2100123 (2 of 8)

ADVANCED
SCIENCE NEWS
www.advancedsciencenews.com

ADVANCED
NANOBIOMED
RESEARCH
Open Access
www.advnanobiomedres.com

Table 1. Chemical compositions of the contrast agents.

Sample ID	NiAl LDH [mg]	MTES [µL]	TEOS [µL]	EtOH [µL]	H$_2$O [µL]	Note
Ref	100	200	50	250	0	Precipitation in >30 min
L0	0	200	50	250	70	No gelation
L10	10	200	50	250	70	Inhomogeneous gelation
L25	25	200	50	250	70	(translucent gel)
L50	50	200	50	250	70	
L75	75	200	50	250	70	Homogeneous gelation
L100	100	200	50	250	70	(transparent gel)
L125	125	200	50	250	70	
L150	150	200	50	250	70	Viscous paste[a)]
L200	200	200	50	250	70	

[a)]Viscous paste formed even before adding H$_2$O, inhibiting the homogenous mixing.

are named as L##, where ## represents the amount of NiAl LDH in Table 1.

The gel was first prepared in a glass pipette to make fundamental characterizations. A photograph of L100, as a representative sample, after gelation is shown in **Figure 2**a. Gelation occurred in 20 min homogenously enough to show optical transparency. No shrinkage of the wet gel, i.e., syneresis, was observed, even 3 months later. This minimal shrinkage is a critical requirement for contrast agents designed to replicate vascular structures. The moderate gelation in 20 min allows for the perfusion process as discussed later.

A XRD pattern of L100 is comparable to that of the freeze-dried LDH precursor, which is ascribed to hydrotalcite-like LDH with rhombohedral (*R3m*) symmetry, as shown in Figure 2b. The values of crystallite size estimated from 003 diffraction using Scherrer's equation are 5.0(3) and 4.4(3) nm for freeze-dried LDH and L100, also suggesting LDH crystals are intact throughout the sol–gel process. To gain better structural insights, the wet gel was subjected to supercritical drying which allows preservation of the original nanostructure of gel networks, and its structural features were closely investigated. Figure 2c,d shows scanning electron microscope (SEM) images of L100 after supercritical drying. The macrostructure is homogenous at µm range (Figure 2c). The gel skeletons were composed of the interconnected primary particles with a diameter of ≈10 nm (Figure 2d). The ordered porosity, as interstices of particles, is also confirmed by N$_2$ adsorption showing a peak centered at 42.3 nm for the pore size distribution (Figure S4, Supporting Information). The mean distance, *h*, between surfaces of neighboring nanoparticles suspended in the precursor solution of L100, is estimated as $h = 4$ nm from Woodcock's equation (Equation 1).[19]

$$h = d_p \left\{ \sqrt{\frac{1}{3\pi F} + \frac{5}{6}} - 1 \right\} \tag{1}$$

where d_p is diameter of particles, F is volume fraction of particles in the precursory solution. Thanks to the extremely small
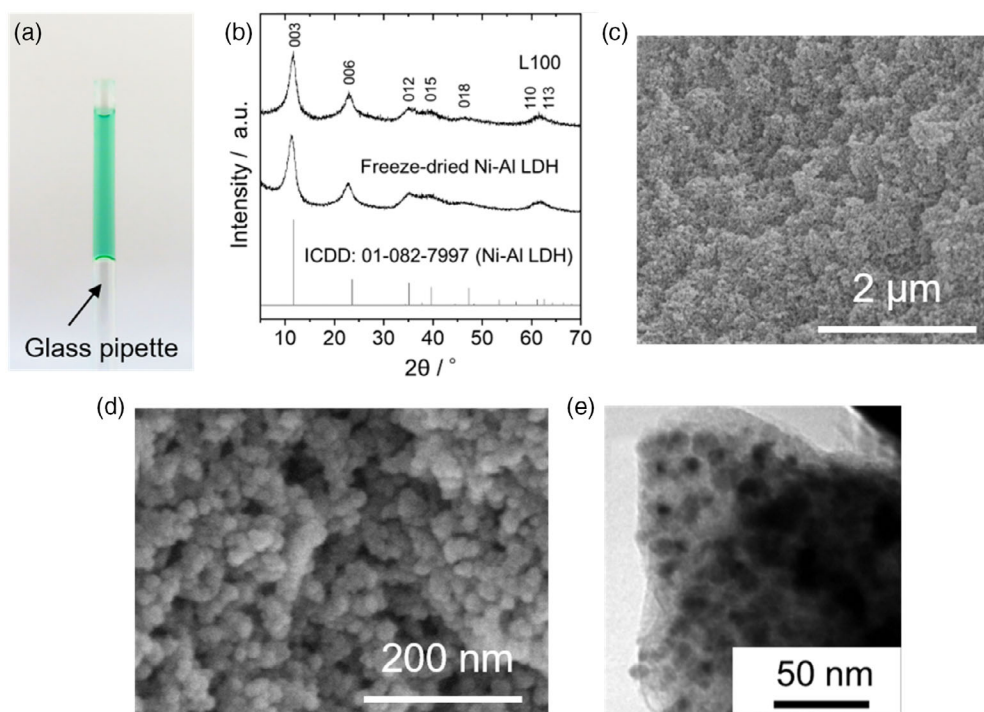

Figure 2. a) Photograph of L100 (wet gel) prepared in a glass pipette with an outer diameter of 1.6 mm. b) XRD patterns of L100 and freeze-dried NiAl LDH powder with reference data (ICDD 01-082-7997). c,d) SEM images and e) TEM image of L100; observations of nanostructures were performed on supercritically dried L100 (aerogel sample).

**ADVANCED
SCIENCE NEWS**

www.advancedsciencenews.com

**ADVANCED
NanoBiomed
RESEARCH**
Open Access

www.advnanobiomedres.com

interparticle distance in the concentrated dispersion, a stimulus to destabilize the dispersion, i.e., in the present case, hydrolysis and condensation reactions of alkoxides on the heterogeneous basic LDH nanocatalyst, can induce gelation. Indeed, transmission electron microscope (TEM) observation revealed that LDH nanoparticles are coated by silica such that nanoparticles are embedded in a film-like silica in the resultant gel matrix (Figure 2e). The atomic ratio of Ni/Si for the aerogel was estimated as 1.3 by the mean of X-ray fluorescence (XRF) analysis, which again supports the formation of the silica and LDH composite.

The first key to the homogenous gelation is a relatively high catalytic activity of the present freeze dried LDH. **Figure 3** shows ^1H NMR spectra of TEOS hydrolyzed with D_2O in the presence of LDH catalysts (details in Supporting Information). The progress of the hydrolysis reaction (conversion, %) was estimated from —CH_2— moieties of $SiOCH_2CH_3$ (precursor) and $DOCH_2CH_3$ (yielded by hydrolysis). This corresponds to the ratio of areas of peaks assigned as H_a and H_c on the spectra. For comparison, three other types of alkalization agents (glycidol, urea, and NaOH) were also employed for LDH synthesis and the

results are summarized in the bottom table of Figure 3. NiAl LDH prepared through epoxide-routes (entry 1 and 4) exhibit catalytic activities, while those prepared with NaOH and urea (entries 2 and 3) show negligible ones. It is apparent that freeze-dried LDH exhibits a relatively high catalytic activity, 88%, among tested samples toward the hydrolysis reaction of TEOS. This is presumably due to the high alkaline nature of LDH prepared though an epoxide-route,[20] rather than nanometric features offering a large surface area. Indeed, specific surface areas of tested samples are comparable, suggesting the different surface natures of those crystals.

The second key to the homogenous gelation is the concentration of the nanoparticles. The homogenous gelation is possible at relatively high LDH concentrations (Table 1). While there have been many reports on LDH/silica composite, they are all obtained as powders rather than monolith demonstrated in the present study.[21] Again, the formation of powders in these previous cases is because the relatively large crystals are synthesized under a diluted condition, whereas the homogeneous interconnection between nanoparticles demonstrated in the present study allows the formation of monolithic materials.

The third key to the homogenous gelation is the elasticity of the obtained materials imparted by the simultaneous use of TEOS and MTES. Elastic gels without any cracks and shrinkage are obtained from the mixture of tetrafunctional and trifunctional alkoxides, TEOS and MTES. The introduction of trifunctional alkoxide imparts an elastic nature due to the polymethylsilsesquioxane networks with a decrease in crosslinking density.[22] Indeed, sample gels with no or less MTES exhibited shrinkage (synersis) and/or cracks in a wet state. While, the inclusion of TEOS (20 vol% in the present study) contributes to improved mechanical strength, such that it can be handled. A higher mechanical strength can be further achieved by increasing LDH content. **Figure 4** shows photographs of solidified contrast agents under loading (tweezer). L25 and L50 were crushed under such minimal loading, while L75 and L100 kept their original shapes. Young's modulus for L75 and L100 were estimated as 25 ± 2.2 and 50 ± 8.7 kPa, respectively, which is a high enough to handle the monolithic gel. The larger mechanical strength with the increase in LDH loading suggests that LDH nanoparticles function as nanofiller to reinforce the silica gel matrix.

In conclusion, we demonstrate here that the concentrated suspension of LDH nanoparticles are a key raw material that allow preparation of a curable inorganic resin with structural homogeneity at μm scale, by integrating with silicon alkoxide-derived sol–gel reaction.
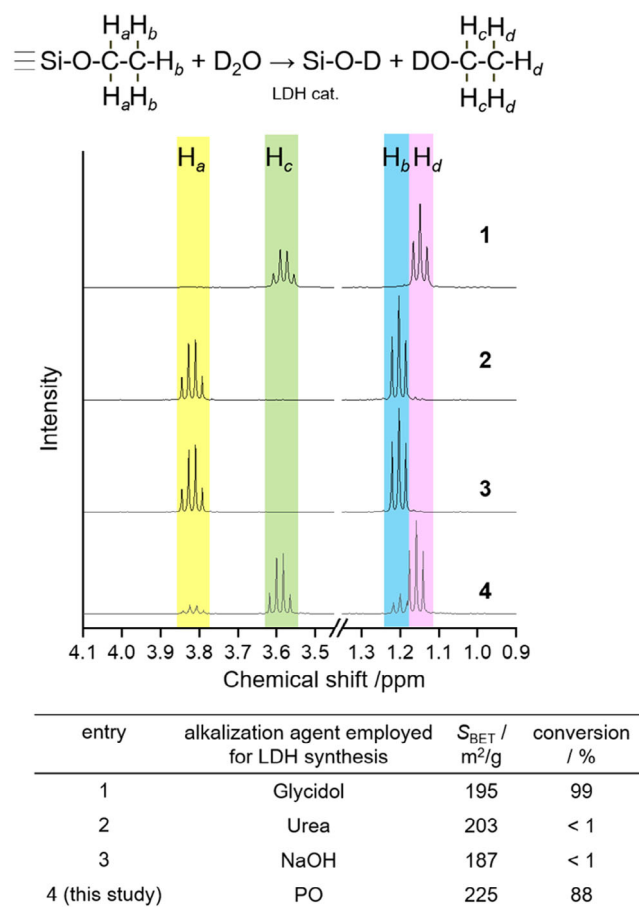

$$\equiv Si-O-\overset{\overset{\displaystyle H_aH_b}{|}}{\underset{\underset{\displaystyle H_aH_b}{|}}{C}}-\overset{\overset{\displaystyle H_b}{|}}{\underset{\displaystyle H_b}{C}}-H_b + D_2O \xrightarrow[\text{LDH cat.}]{} Si-O-D + DO-\overset{\overset{\displaystyle H_cH_d}{|}}{C}-\overset{\overset{\displaystyle H_cH_d}{|}}{C}-H_d$$

entry	alkalization agent employed for LDH synthesis	S_{BET} / m²/g	conversion / %
1	Glycidol	195	99
2	Urea	203	< 1
3	NaOH	187	< 1
4 (this study)	PO	225	88

Figure 3. ^1H NMR spectra and corresponding table for the hydrolysis reaction of TEOS in the presence of various LDH catalysts. Catalytic activity of freeze-dried LDH nanoparticles (entry 4) with a comparison to reference NiAl LDHs prepared by various method (entries 1, 2, and 3). The hydrolysis reaction of TEOS with D_2O was used to assess the reaction rate. Conversion was calculated by peaks derived from protons H_a and H_c.

2.2. Application to Contrast Resin for 3D Tomographic Imaging

The ability of the obtained materials to enhance the X-ray attenuation for μ-CT imaging was systematically evaluated. First, fundamental physical characterizations were performed on the contrast agent prepared in glass capillaries. Detailed procedures for sample synthesis are described in Supporting Information. The contrast agent was introduced into capillaries with diameters of 20, 50, and 100 μm and the samples were analyzed by X-ray μ-CT imaging at the Saga Light Source BL07 with a monochromatic X-ray with a photon energy of 12 keV.
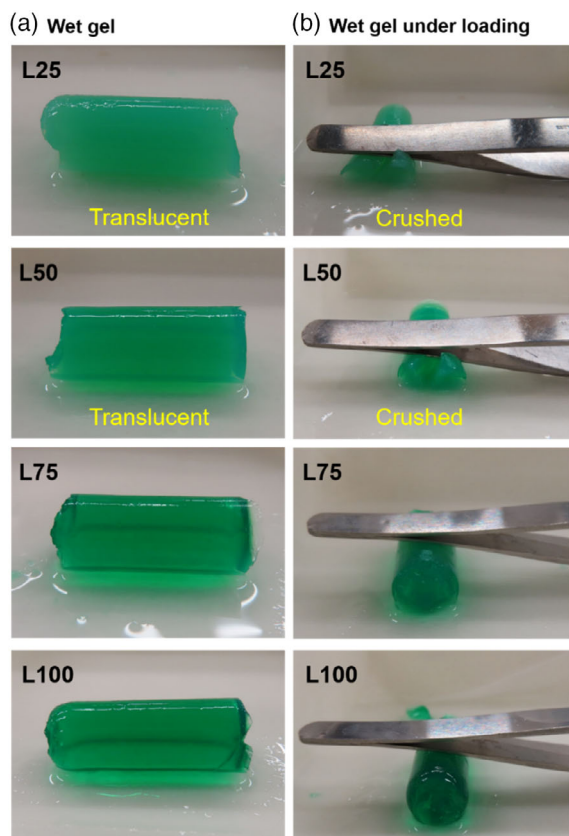
Figure 4. a) Appearance of wet gels prepared at various LDH contents. L25 and L50 are translucent since phase separation occurs in the course of sol–gel reaction. L75 and L100 exhibit optical transparency. b) Photographs of wet gels under loading (17 g tweezers placed on the wet gels).

Figure 5a shows 2D X-ray μ-CT image of L100 prepared in the glass capillary with an inner diameter of 100 μm. Homogeneous contrast was observed throughout the sample. No gaps were observed between contrast agent and silica capillary wall (which can occur as result of shrinkage of contrast agent and/or contamination of bubbles), revealing successful filling of the capillary. The same results were obtained for capillaries with smaller diameters of 20 and 50 μm (Figure S5, Supporting Information). Figure 5b shows X-ray μ-CT images of empty capillary, L50, and L100. High X-ray attenuation of fused silica capillary wall leads to high contrast and this appears white on resulting images, while air appears black due to low X-ray attenuation. Meanwhile, the silica core filled with the contrast agent (wet gel) exhibits higher contrast in comparison to air and this increases with concentration of LDH nanoparticles. The relationship between attenuation coefficient and relative contrast is shown in Figure 5c. As a reference sample, Mercox II kit (Radd research), commercially available contrast agent, was also prepared in the fused silica capillaries. This sample is called as polymethylmethacrylate (PMMA) in this article. The attenuation coefficient was calculated for 12 keV X-ray energy from the chemical composition (ratios of constituent elements) by setting a density of $0.97 \, g \, cm^{-3}$ for the resins (wet gels); the value was experimentally obtained for L100. The attenuation coefficient
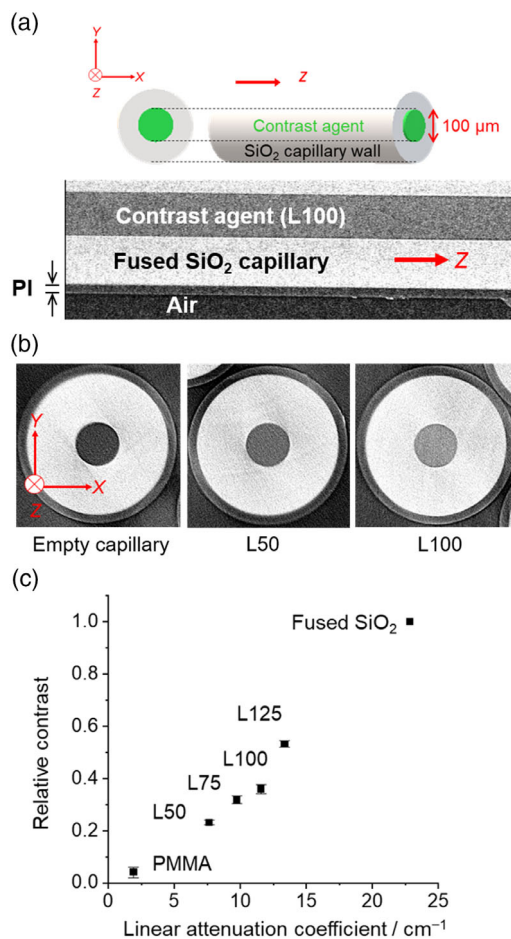

Figure 5. a) 2D X-ray μ-CT image of L100 prepared in the silica capillary. The inner and outer diameters of silica capillary are 100 and 375 μm, respectively. b) 2D X-ray μ-CT images for empty capillary, L50, and L100. c) Relationship between linear attenuation coefficient and relative contrast. The contrast of fused SiO_2 (silica capillary wall) was used as a standard, and set at relative contrast of 1. PI: polyimide coating made on the outer surface of the capillaries.

increases linearly with increasing LDH concentration, suggesting that LDH nanoparticles successfully attenuate X-rays to enhance the contrast of the resins. Although L125 exhibited the best contrast among the samples tested, its viscosity was relatively high compared with the other compositions (Figure S6, Supporting Information). L100 and other samples with lower LDH contents exhibits lower shear viscosity compared with PMMA. The lower viscosity is favorable for the perfusion process. The L100 sample is a good compromise exhibiting a relatively low viscosity compared with PMMA and high contrast. It should be noted that the viscosity of contrast agents increases once polymerization reactions start. The progress of polymerization and the resultant gelation time for LDH based contrast agents can be tuned by titrating the chemical compositions (mole ratio of tri- and tetra-functionalized alkoxide) and/or practical replacement of ethanol solvent with other alcohols. For example, the replacement of the ethanol solvent with methanol prolongs the gelation time; the full replacement of ethanol results in gelation in >5 h. The amount of H_2O added as a gelation initiator

also influences on the gelation time, while the gelation time is more strongly depend on the composition of the solvent in the current nanoparticulate-based sol-gel system.

Resin composition L100 was employed in the perfusion of blood vessels in two use cases (**Figure 6**; human placenta and murine liver) to demonstrate the applicability and performance of the material systems developed here. Perfusion of L100 was relatively easy compared with PMMA due to the lower viscosity. The green color of the LDH aerogel resin allowed for visual identification of the sections of the tissue and organs successfully perfused (Figure 6Ai) thus guiding sectioning prior to imaging. Synchrotron µCT imaging was performed at the Diamond Light Source I13-2 beamline and images processed using Avizo commercial software (Thermo Fisher Scientific). Images of the tissue digital cross sections show L100 perfused vessels have high contrast in comparison to surrounding tissue (Figure 6 Aii and Bi), facilitating relatively straightforward segmentation based on the contrast. Importantly, segmentation of the blood vessels was performed without the need for maceration of the surrounding tissue.
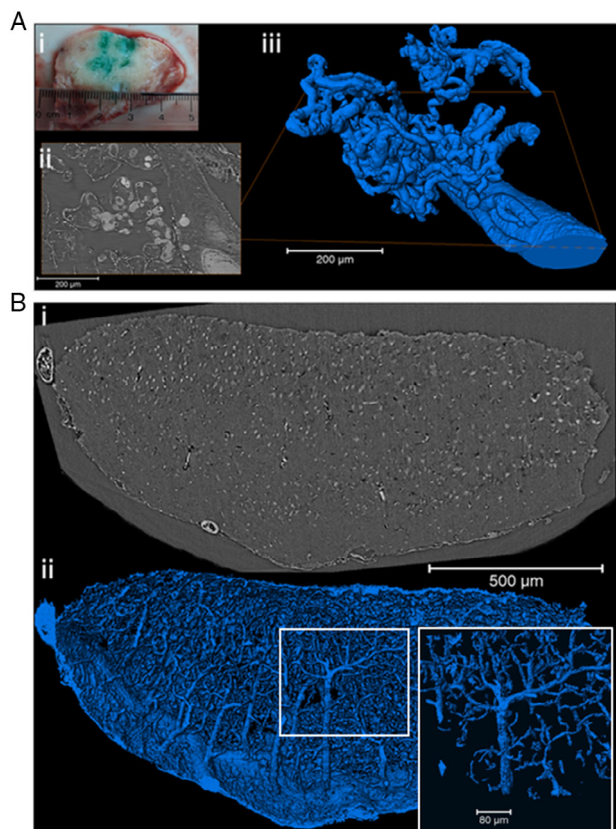
Figure 6Aiii shows 3D rendering of the L100-perfused fetal blood vasculature from a human placenta. Capillary loops within a terminal villi have been successfully perfused, suggesting that L100 has sufficiently low viscosity to allow entry to the smallest vessels having a diameter of 5 µm. However, only a small section of the fetal vasculature is perfused, as evident from Figure 6Aii which shows a large number of terminal villi containing no L100. This could be due to several reasons, including insufficient amount of L100 perfused and lack of access to the villi network from limitation of the cannulation method employed. Conversely, the murine liver, which was perfused via the heart, appears to have been successfully perfused. The various vascular trees originating from the bottom wall of the liver, which extend and branch out within it, are very well perfused with L100 (Figure 6Bii). This suggests that L100 is a suitable contrast agent for µCT and should allow blood vasculature to be imaged and quantified both in human and animal tissues and organs.

3. Conclusion

A curable inorganic resin with structural homogeneity at µm scale has been developed by integrating concentrated dispersion of NiAl LDH with silicon alkoxide-derived sol–gel reaction. The gelation is induced by the relatively high catalytic activity of the present NiAl LDH nanoparticles. The high concentration of NiAl LDH nanoparticles of the dispersion also contributed to form a monolithic gel. Sample gels with no or less MTES exhibited shrinkage (syneresis) and/or cracks in a wet state. While, the inclusion of TEOS (20% vol in the present study) improves mechanical strength, such that it can be handled. The X-ray attenuation coefficient of contrast agents in glass capillaries increases linearly with increasing LDH concentration. L100 sample, whose composition is 100 mg NiAl LDH, 200 µL MTES, 50 µL TEOS, 250 µL EtOH, and 70 µL H_2O, is a good compromise exhibiting a relatively low viscosity compared with PMMA and high contrast. As a proof-of-concept, we have applied it to maceration-free X-ray µ-CT imaging of blood vessels of a human placenta and murine liver. Imaging and quantification of blood vasculature both in human and animal tissues and organs have been successfully demonstrated. This contrast agent is readily prepared and used and therefore provides a promising option for imaging, allowing high contrast, which has the potential to offer deeper insights into vascular pathology.

4. Experimental Section

Synthesis of Precursory Ni-Al LDH Powders: $NiCl_2 \cdot 6H_2O$ (1.188 g; 5.000 mmol) and $AlCl_3 \cdot 6H_2O$ (0.604 g; 2.500 mmol) were dissolved in a mixture of ethanol (EtOH, 3.00 mL; 51.4 mmol) and distilled water (2.00 mL; 111 mmol), followed by the addition of acetylacetone (acac, 260 µL; 2.53 mmol). After the mixture was stirred for >30 min in a glass closed container at a room temperature (≈25 °C), propylene oxide (PO, 2.62 mL; 37.4 mmol) was added to the mixture and stirred for a further 1 min to yield a homogeneous solution. The container was sealed and stored at a room temperature (≈25 °C). After 24 h, the NiAl LDH suspension was poured on a petri dish and cooled in a freezer at −20 °C. Then, the petri dish was covered with an Al foil with holes, and placed in a freeze dryer equipped with a dry chamber (FDS-1000 and DRS-2, EYELA, Japan). (Note: the ethanolic aqueous solution boils under the reduced pressure.

Figure 6. Example use cases for the perfusion and contrast enhancement by L100. (Ai) Photo of a section of a human placenta infused with L100 showing its green color in parts of the tissue. Cross sectional slices obtained from the synchrotron sourced µCT dataset on (Aii) human placenta and (Bi) murine liver, showing the high contrast on L100 in the blood vessels. The L100 enabled contrast-based segmentation of the blood vessels and 3D rendering of the blood vessels to be produced for (Aiii) human placenta and (Bii) murine liver, and inset shows zoomed in images of a single tree.

The cover of Al foil is required to prevent samples from flying off upon drying.) The drying was performed overnight under a reduced pressure of <10 Pa. The freeze-dried LDH powder was collected and used as a nanoparticulate precursor to prepare contrast agents.

Synthesis of Contrast Agent: TEOS, MTES, and EtOH were mixed. The freeze-dried NiAl LDH powder was added to the mixture to form a homogeneous colloidal suspension (Note: the suspension should be used within 30 min. Aggregation of the particles gradually occur in longer time). Then, H_2O was added and further stirred for 1 min to give the contrast agent. Immediately after, the reacting contrast agent was injected in a silica glass tubes or capillaries, and placed at 37 °C, or perfused in blood vessels (details on perfusion procedure is given in imaging section). The chemical compositions of the contrast agents are summarized in Table 1. For field emission scanning electron microscope (FE-SEM) and transmission electron microscope (TEM) observations, the solidified contrast agent (wet gel) was submerged in abundant isopropyl alcohol at a room temperature for 24 h to exchange the solvent, followed by CO_2 supercritical drying at 80 °C 14 MPa.

Characterization: The crystalline nature of samples was identified by powder X-ray diffraction (PXRD; MiniFlex-II, Rigaku Corp., Japan) using Cu Kα radiation ($\lambda = 0.1540$ nm) equipped with a graphite monochrometer. Divergence and scattering slits (DS and SS) were set at 1.25°, and receiving slit was set at 0.3 mm. Crystallite size (D) was estimated with Scherrer's equation, $D = K\lambda/(B\cos\theta)$. Here, λ is the wavelength of Cu Kα radiation (0.154 nm) and θ is Bragg's angle. B was set as an integral breadth of the diffraction peak and K was set as a constant of 4/3. N_2 adsorption–desorption isotherms at −196 °C were obtained on a volumetric gas adsorption apparatus (BELSORP-mini II, Microtrac BEL Corp., Japan) for the samples heated at 300 °C for 8 h. Prior to the measurements, sample powders were pretreated at 200 °C under a vacuum condition overnight. Specific surface area (S_{BET}) of catalysts was estimated by the Brunauer–Emmett–Teller (BET) method. Morphologies and sizes of the samples were investigated by a FE-SEM (S-4800, Hitachi Corp., Japan, with a thin Pt coating) and a TEM (JEM-2000FX, JEOL Ltd., Japan). The sample for TEM observation was ground to disperse in 2-propanol and the supernatant was dropped onto a Cu grid. The chemical compositions of the resultant LDH-based contrast agents were determined by XRF (EDX-7000 Shimadzu Corp., Japan), based on a calibration-curve-method (see Supporting Information). The viscosity of the samples, before the initiation of gelation, was measured by a rheometer in the cone-and-plate geometry (Modular Compact Rheometer MCR102, Anton Paar GmBH, Austria). The measurements of FE-SEM, TEM, N_2 adsorption–desorption, and XRF were performed on the LDH-based contrast agent aged for 1 week to ensure completion of the sol–gel reaction. Liquid ^1H NMR spectra were recorded using an NMR spectrometer (JNM-ECX 400 and JNX-ECS 400, JEOL Ltd., Japan). ^1H NMR spectroscopy was used to estimate catalytic activities of various LDHs. Further details are described in Supporting Information. Young's modulus of the solidified contrast agent (wet gel) was estimated by compression testing with a universal tester (EZ-SX, Shimadzu Corp., Japan).

3D Tomographic Imaging: Two use cases (human placenta and murine liver) were employed to evaluate blood vessel perfusion and contrast enhancement. L100 compositions was prepared as outlined in section "Synthesis of Contrast Agent" and perfused following preparation of placenta or mice. Within the placenta the fetal side was perfused with L100 while in the mice, the entire animal blood vasculature was perfused via the heart.

Human placenta acquired from full-term placentas delivered at St Mary's Hospital, Manchester, UK, with appropriate informed written consent and ethical approval provided by North West - Greater Manchester West Research Ethics Committee (Tommy's Project REC 15/NW/0829) were perfused and prepared following procedure described.[3] Briefly, collected placentas were cannulated using a glass capillary via chorionic plate artery and vein within an intact cotyledon and perfused with a modified Earle's bicarbonate buffer at 6 mL min^{-1}. The maternal-side was cannulated at the center of a placental cotyledon and perfused with the same buffer at 14 mL min^{-1} for 3 h. The cotyledon was then perfusion fixed from the maternal-side with Zinc 7 fixative[23] for 15 min. Immediately after,

L100 was infused into the fetal side. A $5 \times 5 \times 5$ mm^3 section of the perfused and L100 infused cotyledon was dissected and further fixed in a PFA fixative overnight then wax embedded before CT imaging.

Mice (24 week old, male, C57Bl/6J) were purchased from the Jackson Laboratory and bred and housed at a barrier and specific pathogen-free facility at the Biomedical Services Unit, University of Birmingham (Birmingham, UK) under license number PFBB3DA4C. Mice were sacrificed using a rising concentration of CO_2 and, following confirmation of death, a lateral incision was made just below the ribcage and a hole was made in the diaphragm to expose the heart. The carotid artery was also cut to allow blood to drain during perfusion. Mice were perfused through the left atrium using a 21 gauge needle with 5 mL modified Earle's bicarbonate buffer (as above) followed by 12 mL L100. Once 15 min has elapsed (to ensure polymer setting), tissues for imaging were then removed and fixed in 4% PFA overnight and then dehydrated by sequential submersion in ethanol (70%, 95%, and 100%). Tissues for imaging were then removed and fixed in 4% PFA prior to imaging. All experiments were performed under guidelines of, and were approved by, the UK Home Office and the Animal Welfare Ethical Review Body (AWERB) of the University of Birmingham.

Contrast agent-infused tissues were imaged at Diamond Light Source (DLS) facility (Harwell, UK; Manchester Imaging Branchline, I13-2). High-resolution synchrotron-sourced in-line phase contrast microcomputed X-ray tomography was used to generate 3D images. Briefly, polychromatic X-ray beams with energy in the range of 8–30 keV was filtered (1.3 mm pyrolytic graphite and 3.2 mm Al filters) and directed at the samples. A scintillator coupled (500 μm thick CdWO4) sCMOS detector (2560 × 2160 px; pco.edge 5.5; PCO AG, Germany) positioned between 60 and 100 mm away, in-line with the sample, was used to capture the transmitted X-rays. The light was then magnified with various objectives to result in an effective isotropic pixel size of 0.81 μm. A total of 3001–4001 projections were recorded over 0°–180° rotation using exposure times between 80 and 200 ms. These were then reconstructed into 3D datasets using a filtered back projection algorithm[24] incorporating dark- and flat-field correction, ring artefact suppression and lens blurring.[25]

3D tomographic imaging for fundamental examinations was also performed at BL-07 with a monochromatized synchrotron X-ray with an energy of 12 keV.[26] The samples in capillaries were placed on rotationary stage and transmitted X-rays were detected by a micro-X-ray camera (Kenvy-2) composed of CsI scintillator (1 mm thickness), 5× objective lens, and sCMOS (2048 pixel × 2048 pixel). The optical magnification of 5× employed results in an effective isotropic pixel size of 1.3 μm. In total, 1000 X-ray projections were recorded over 0°–360° rotation. Projections were reconstructed into 3D datasets using a filtered back projection algorism using a Shepp-Logan filter. The relative contrast was evaluated with ImageJ. The linear attenuation coefficient at 12 keV was estimated from the Victoreen equation with setting the ratio of the elements and setting a density of 0.97 g cm^{-3} for the resins; the value was experimentally obtained one for L100.

Statistical Analysis: For the measurement of Young's modulus, the samples were prepared to have a cylindrical shape of 13–14 mm in diameter and 5–7 mm in height. Greater than four specimens were tested for each sample, and the values were represented as mean ± SD. Relative contrast (Figure 5) is plotted as mean ± SD, as a function of linear attenuation coefficient.

Supporting Information

Supporting Information is available from the Wiley Online Library or from the author.

Acknowledgements

Conflict of Interest

The authors declare no conflict of interest.

Data Availability Statement

Research data are not shared.

Keywords

[1] E. Meijering, A. E. Carpenter, H. Peng, F. A. Hamprecht, J. C. Olivo-Marin, *Nat. Biotechnol.* **2016**, *34*, 1250.

[2] a) D. P. Cormode, P. C. Naha, Z. A. Fayad, *Contrast Media Mol. Imaging* **2014**, *9*, 37; b) E. N. Landis, D. T. Keane, *Mater. Charact.* **2010**, *61*, 1305.

[3] W. M. Tun, G. Poologasundarampillai, H. Bischof, G. Nye, O. N. F. King, M. Basham, Y. Tokudome, R. M. Lewis, E. D. Johnstone, P. Brownbill, M. Darrow, I. L. Chernyavsky, *J. R. Soc., Interface* **2021**, *18*, 20210140.

[4] a) C. Debbaut, P. Segers, P. Cornillie, C. Casteleyn, M. Dierick, W. Laleman, D. Monbaliu, *J. Anat.* **2014**, *224*, 509; b) W. L. Mondy, D. Cameron, J. P. Timmermans, N. De Clerck, A. Sasov, C. Casteleyn, L. A. Piegl, *Tissue Eng., Part C* **2009**, *15*, 729; c) C. Debbaut, J. Vierendeels, C. Casteleyn, P. Cornillie, D. Van Loo, P. Simoens, L. Van Hoorebeke, D. Monbaliu, P. Segers, *J. Biomech. Eng.* **2012**, *134*, 011003.

[5] a) C. King, W. Birch, *J. Forensic Sci.* **2015**, *60*, 124; b) A. J. Miodoński, J. A. Litwin, *Anat. Rec.* **1999**, *254*, 375; c) I. A. Bhutto, T. Amemiya, *Anat. Rec.* **2001**, *264*, 63; d) F. D. Verli, T. R. Rossi-Schneider, F. L. Schneider, L. S. Yurgel, M. A. L. De Souza, *Scanning* **2007**, *29*, 128; e) H. Zhao, J. Azuma, F. Kalish, R. J. Wong, D. K. Stevenson, *Biol. Reprod.* **2011**, *85*, 1005.

[6] A. L. Bernstein, A. Dhanantwari, M. Jurcova, R. Cheheltani, P. C. Naha, T. Ivanc, E. Shefer, D. P. Cormode, *Sci. Rep.* **2016**, *6*, 26177.

[7] a) X. Chenjie, G. A. Tung, S. Shouheng, *Chem. Mater.* **2008**, *20*, 4167; b) Q. Y. Cai, S. H. Kim, K. S. Choi, S. Y. Kim, S. J. Byun, K. W. Kim, S. H. Park, S. K. Juhng, K. H. Yoon, *Invest. Radiol.* **2007**, *42*, 797;

[8] H. Kamiya, Y. Otani, M. Fuji, M. Miyahara, in *Nanoparticle Technology Handbook* **2018**, p. 109.

[9] Z. P. Xu, N. D. Kurniawan, P. F. Bartlett, G. Q. Lu, *Chem. - Eur. J.* **2007**, *13*, 2824.

[10] W. Xie, Z. Guo, Z. Cao, Q. Gao, D. Wang, C. Boyer, M. Kavallaris, X. Sun, X. Wang, L. Zhao, Z. Gu, *ACS Biomater. Sci. Eng.* **2019**, *5*, 2555.

[11] a) P. R. Wei, S. H. Cheng, W. N. Liao, K. C. Kao, C. F. Weng, C. H. Lee, *J. Mater. Chem.* **2012**, *22*, 5503; b) Y. M. Kuo, Y. Kuthati, R. K. Kankala, P. R. Wei, C. F. Weng, C. L. Liu, P. J. Sung, C. Y. Mou, C. H. Lee, *J. Mater. Chem. B* **2015**, *3*, 3447.

[12] S. Y. Jung, G. H. Gwak, J. K. Park, J. M. Oh, *RSC Adv.* **2020**, *10*, 5838.

[13] L. Wang, H. Xing, S. Zhang, Q. Ren, L. Pan, K. Zhang, W. Bu, X. Zheng, L. Zhou, W. Peng, Y. Hua, J. Shi, *Biomaterials* **2013**, *34*, 3390.

[14] B. Li, J. Tang, W. Chen, G. Hao, N. Kurniawan, Z. Gu, Z. P. Xu, *Biomaterials* **2018**, *177*, 40.

[15] a) W. Xie, Z. Guo, Q. Gao, D. Wang, K. Liang, Z. Gu, L. Y. Zhao, *ACS Appl. Bio Mater.* **2020**, *3*, 5845; b) H. Zuo, W. Chen, B. Li, K. Xu, H. Cooper, Z. Gu, Z. P. Xu, *Chem. - Eur. J.* **2017**, *23*, 14299.

[16] M. S. Usman, M. Z. Hussein, A. U. Kura, S. Fakurazi, M. J. Masarudin, F. F. Ahmad Saad, *Mater. Chem. Phys.* **2020**, *240*, 122232.

[17] Y. Tokudome, T. Morimoto, N. Tarutani, P. D. Vaz, C. D. Nunes, V. Prevot, G. B. G. Stenning, M. Takahashi, *ACS Nano* **2016**, *10*, 5550.

[18] a) Z. Liu, R. Ma, M. Osada, N. Iyi, Y. Ebina, K. Takada, T. Sasaki, *J. Am. Chem. Soc.* **2006**, *128*, 4872; b) Z. P. Xu, G. Stevenson, C. Q. Lu, G. Q. Lu, *J. Phys. Chem. B* **2006**, *110*, 16923; c) Z. P. Xu, G. S. Stevenson, C. Q. Lu, G. Q. Lu, P. F. Bartlett, P. P. Gray, *J. Am. Chem. Soc.* **2006**, *128*, 36; d) G. Layrac, M. Destarac, C. Gérardin, D. Tichit, *Langmuir* **2014**, *30*, 9663; e) Z. Gu, H. L. Zuo, L. Li, A. H. Wu, Z. P. Xu, *J. Mater. Chem. B* **2015**, *3*, 3331.

[19] M. Iijima, M. Tsukada, H. Kamiya, *J. Colloid Interface Sci.* **2007**, *307*, 418.

[20] Y. Tokudome, M. Fukui, S. Iguchi, Y. Hasegawa, K. Teramura, T. Tanaka, M. Takemoto, R. Katsura, M. Takahashi, *J. Mater. Chem. A* **2018**, *6*, 9684.

[21] a) M. Mishra, M. R. Das, R. L. Goswamee, *J. Sol-Gel Sci. Technol.* **2010**, *54*, 57; b) J. Liu, R. Harrison, J. Z. Zhou, T. T. Liu, C. Yu, G. Q. Lu, S. Z. Qiao, Z. P. Xu, *J. Mater. Chem.* **2011**, *21*, 10641; c) L. Wang, J. Shi, Y. Zhu, Q. He, H. Xing, J. Zhou, F. Chen, Y. Chen, *Langmuir* **2012**, *28*, 4920; d) S. D. Jiang, Z. M. Bai, G. Tang, L. Song, A. A. Stec, T. R. Hull, Y. Hu, W. Z. Hu, *ACS Appl. Mater. Interfaces* **2014**, *6*, 14076; e) X. Ji, W. Zhang, L. Shan, Y. Tian, J. Liu, *Sci. Rep.* **2015**, *5*, 18367; f) S. Zhao, W. C. Tsen, F. Hu, F. Zhong, H. Liu, S. Wen, G. Zheng, C. Qin, C. Gong, *J. Mater. Sci.* **2020**, *55*, 2967.

[22] K. Kanamori, K. Nakanishi, *Chem. Soc. Rev.* **2011**, *40*, 754.

[23] D. Lykidis, S. Van Noorden, A. Armstrong, B. Spencer-Dene, J. Li, Z. Zhuang, G. W. H. Stamp, *Nucleic Acids Res.* **2007**, *35*, e85.

[24] A. C. Kak, M. Slaney, *Principles of Computerized Tomographic Imaging*, Society for Industrial and Applied Mathematics, Philadelphia **2001**.

[25] a) R. C. Atwood, A. J. Bodey, S. W. T. Price, M. Basham, M. Drakopoulos, *Philos. Trans. R. Soc., A* **2015**, *373*, 20140398; b) M. C. Strotton, A. J. Bodey, K. Wanelik, M. C. Darrow, E. Medina, C. Hobbs, C. Rau, E. J. Bradbury, *Sci. Rep.* **2018**, *8*, 12017.

[26] A. Yoneyama, R. Baba, M. Kawamoto, *Opt. Mater. Express* **2021**, *11*, 398.